Experiments in Fluids 25 (1998) 42–49 © Springer-Verlag 1998

Experimental investigation on turbulent flow in a circular-sectioned 90-degree bend

K. Sudo, M. Sumida, H. Hibara

Abstract The steady, turbulent flow in a circular-sectioned 90° bend with smooth walls has been investigated experimentally. The bend had a curvature radius ratio of 4.0 with long, straight upstream and downstream pipes. The longitudinal, circumferential and radial components of mean and fluctuating velocities, and the Reynolds stresses in the pipe cross section at several longitudinal stations were obtained with the technique of rotating a probe with an inclined hot wire at a Reynolds number of 6×10^4. The velocity fields of the primary and secondary flows, and the Reynolds stress distributions in the cross section were illustrated. Moreover, other characteristics of the bend flow, such as deviation of the primary flow and intensity of the secondary flow, were presented. Simultaneously, discussions were given on the transition of phenomena in the longitudinal direction and the structures of turbulence in the 90° bend.

List of symbols

C_p	pressure coefficient, $C_p = (p - p_{\mathrm{ref}})/(\rho Wa^2/2)$
d	pipe diameter, $d = 2a = 104$ mm
h	$h = Rc + r \sin\theta$
I_s	intensity of secondary flow, see Eq. (5)
k_a	turbulence intensity, see Eq. (6)
p	static pressure at wall
p_{ref}	reference value of p, i.e., p at $z'/d = -17.6$
P_{ww}, P_{wu}, P_{vw}	production rates of Reynolds stresses $\overline{w'^2}$, $\overline{w'u'}$, $\overline{v'w'}$, respectively
R_c	bend curvature radius, $R_c = 208$ mm
Re	Reynolds number, $Re = Wad/\nu$
$\bar{U}$, $\bar{V}$, $\bar{W}$	time mean velocities in r, θ, $\varphi(z)$ directions, respectively
u', v', w'	fluctuating velocities in r, θ, $\varphi(z)$ directions, respectively
Wa	spatial mean velocity, $Wa = 8.7$ m/s
r, θ, $\varphi(z)$	radial, circumferential and longitudinal coordinates
$\bar{x}$	deflection of longitudinal flow, see Eq. (4)
z, z'	longitudinal distance along pipe axis
ν	kinematic viscosity of fluid
ρ	density of fluid

Received: 21 April 1997/Accepted: 14 November 1997

K. Sudo, M. Sumida, H. Hibara
Faculty of Engineering, Hiroshima University
1-4-1, Kagamiyama, Higashihiroshima, 739-8527, Japan

Correspondence to: K. Sudo

1 Introduction

Flows in curved pipes occur in various engineering devices such as piping systems of industrial plants, fluid turbomachinery and heat exchangers. Since such flows are often turbulent, a number of investigations of turbulent flow in curved pipes have been made by measuring the pressure losses with various pressure gages and the velocities with a Pitot tube, and by visualizing the velocity field. Recently, owing to the development of measuring devices and/or by request of workers constructing a numerical turbulence model, experimental studies have been encouraged to understand, in greater detail, the physical mechanisms of turbulent flow through curved pipes. There are several representative investigations of early studies on curved ducts, e.g., those by Humphrey et al. (1981), Taylor et al. (1982) and Chang et al. (1983). Humphrey et al. (1981) and Taylor et al. (1982) measured the velocities of water flowing through a square-sectioned 90° bend with a 4.5 radius ratio, which is the magnitude of the mean curvature radius to the half hydraulic diameter of the bend, using laser doppler velocimetry, and they provided detailed results including Reynolds stresses. Chang et al. (1983) also presented experimental data for a rectangular-sectioned 180° bend with a radius ratio of 6.75.

However, there are few works on turbulent flows in bends with a circular cross section, which seems to be the most important in practical use, except for the measurements of water flows obtained using laser doppler velocimetry by Enayet et al. (1982) and Azzola et al. (1986). Longitudinal mean and fluctuating velocities were measured in a 90° bend with a radius ratio, R_c/a, of 5.58 at a Reynolds number of 43000 by Enayet et al., and in a 180° bend with $R_c/a = 6.75$ at $Re = 57400$ and 110000 by Azzola et al. Unfortunately, these data are limited only to the longitudinal direction. More detailed experimental information is needed to construct the mathematical models of turbulence for numerical computation and to understand the physical phenomena of curved pipe flows.

The purpose of this paper is to provide detailed information on turbulent flow through a circular-sectioned 90° bend with strong curvature.

2 Experimental apparatus and procedures

The experimental apparatus is illustrated schematically in Fig. 1, together with the coordinate system adopted. It is

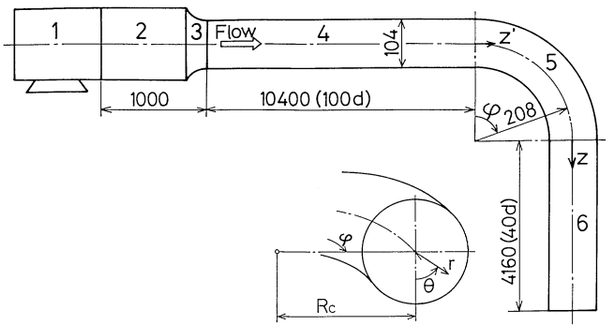

Fig. 1. Schematic diagram of test pipe and coordinate system. *1* Fan; *2* settling chamber; *3* contraction; *4* upstream tangent; *5* 90° bend; *6* downstream tangent

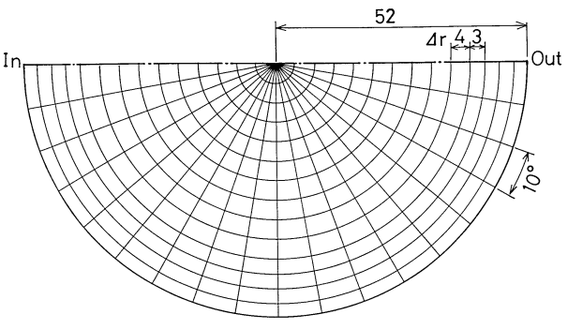

Fig. 2. Measuring points

composed of a 90° bend of curvature radius $R_c = 208$ mm, upstream and downstream tangents of 10.4 ($z'/d = -100$) and 4.16 m ($z/d = 40$), and a settling chamber for air flow discharged from a forced draft fan. The bend is manufactured from acrylic blocks and the two tangents are made of transparent glass. The configuration of the test pipe is circular and its inner diameter, d, is 104 mm. The radius ratio of the bend, R_c/a, is 4, where a is the radius of the pipe. The bend was set in the horizontal plane (see Fig. 1).

Measurements were performed for an air flow with the bulk mean velocity $Wa \fallingdotseq 8.7$ m/s, it corresponding to a Reynolds number of 60000, which was chosen with reference to the previous works of Enayet et al. (1982) and Azzola et al. (1986). Velocity measurements were made by rotating a single inclined hot wire. This method is a more suitable one, under the present circumstances, than LDV for obtaining the time-averaged and fluctuating velocities in three directions and the Reynolds stresses corresponding to them. The details on the method of measuring the velocity data are described in the work by Sudo et al. (1992). Preliminary measurements were obtained at $\varphi = 60°$ in the bend, as well as at $z'/d = -1$ and $z/d = 5$ in the upstream and downstream tangents, to evaluate the symmetry of the flow. For this symmetry confirmation, measurements of the mean and fluctuating velocities were made in the lower half of the cross section of the pipe. Seventeen stations between $z'/d = -1$ and $z/d = 10$ were selected for velocity measurements. The data at each station were obtained at 266 ($= 19 \times 14$) points which correspond to the nodes of the meshes made by dividing half the cross section of the pipe, see Fig. 2. This choice of the nonuniform mesh size is based on the fact that physically, drastic velocity changes occur near the pipe wall; Δr should be made small near the wall but can be made moderately large in the neighborhood of the center of the pipe. In addition to the velocity measurements, the static pressure was measured on the pipe wall between the upstream and the downstream tangents including the bend.

The results of the velocity obtained at the station $z'/d = -1$ in the upstream tangent are in good agreement with the data obtained by Laufer (1954) for a straight pipe. This suggests that a fully developed turbulent current flows into the bend. The measurement uncertainty, the determination of which is described in ANCI/ASME PTC 19.1 (1987), of the present data is $\pm 2.9\%$ for the mean velocity and $\pm 4.1\%$ for the dual and cross correlations of the fluctuating velocity. The estimates of systematic and random errors and the corresponding uncertainties for variables are summarized in Table 1.

Table 1. Measurement errors (%)

Quantity	Systematic error	Random error	U_{RSS}
Wa	± 0.2	± 0.5	± 1.02
$\bar{U}, \bar{V}, \bar{W}$	± 0.2	± 1.44	± 2.9
$\overline{u'^2}, \overline{v'^2}, \overline{w'^2}, \overline{w'u'}, \overline{v'w'}$	± 0.2	± 2.05	± 4.1
P_{ww}, P_{wu}, P_{vw}	± 0.2	± 4.5	± 9.0
$\bar{x}/d$	± 0.3	± 1.5	± 3.0
I_s	± 0.3	± 3.1	± 6.2
k_a	± 0.3	± 4.8	± 9.6

3 Results and discussion

3.1 Mean velocities

The wall static pressure at various θ is plotted against the longitudinal distance, z, in the form of the pressure coefficient C_p, in Fig. 3. Distributions of the longitudinal and circumferential mean velocity components in the horizontal and vertical plane are shown in Fig. 4. Contours of longitudinal mean velocity and velocity vectors of secondary flow at successive longitudinal stations are also provided in Fig. 5.

At $z'/d = -1$, the flow is not yet influenced by the bend and the contours are concentric circles. At the inlet plane of the bend, $\varphi = 0°$, the fluid is slightly accelerated near the inner wall in accordance with the initially favourable longitudinal pressure gradient there (see Fig. 3). Simultaneously, the fluid near the outer wall is decelerated according to the initially unfavourable pressure gradient. This induces a secondary flow towards the inner wall over the entire cross section. At $\varphi = 30°$, the well-known secondary flow due to the centrifugal force appears in the cross section and it forms two counterrotating vortices that circulate outwards in the central part of the pipe and inwards near the upper and lower walls. The fluid with fast longitudinal velocity, however, moves near the inner wall of the bend, as before. At $\varphi = 60°$, the faster fluid near the inner wall is transported by the secondary flow towards the outer wall through the central region of the cross section. The slower fluid near the upper and lower wall, in return, is convected towards

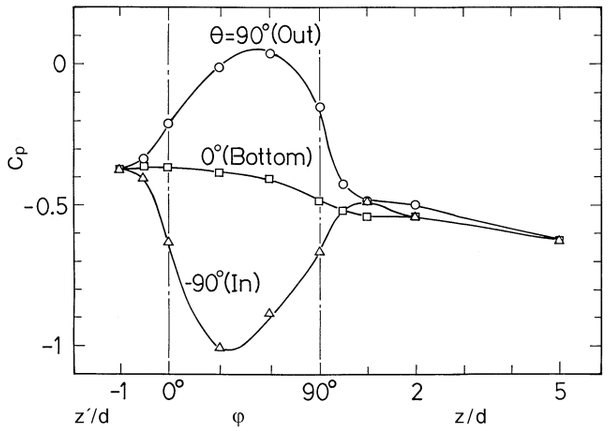

Fig. 3. Longitudinal distribution of wall static pressure

the inner wall side along the wall by the secondary flow. Since the pressure at this station, moreover, increases near the inner wall in the longitudinal direction, the fluid near the inner wall begins to decelerate. The secondary flow grows up rapidly near this station, as illustrated later in Fig. 9. Thereafter the fast fluid in the primary flow moves further towards the outer wall along the symmetric horizontal plane of the bend due to the strong secondary flow. From $\varphi=75^\circ$ to $\varphi=90^\circ$, the fast fluid conveyed to the outer wall is carried towards the inner wall by the secondary flow moving inwards along the wall. This results in greatly distorted velocity contours which are tongue-shaped and enclose the low-velocity region near the inner wall.

Between $z/d=0.5$ and 1, the fluid with low velocity near the inner wall observed at $\varphi=90^\circ$ shifts towards the central region of the pipe due to the outward secondary flow and a depression is formed in the contour plot between the inner wall and the center region of the bend. This depression, which is also observed near the exit plane of the bend, was found in the measurements by Enayet et al. (1982). Meanwhile the strong unfavourable longitudinal pressure gradient in the inner wall side decreases and the fluid there gradually accelerates. Therefore the longitudinal velocity of the fluid increases near the inner wall. For $z/d=2$ to 5, the depression in the contours moves farther towards the outer wall, and the secondary flow weakens gradually, its cores shifting to the central part of the pipe. Further downstream, at $z/d=10$, the secondary flow, in the form of a vortex, breaks down and the longitudinal velocity shows a smooth profile without unevenness. However, a further longitudinal distance is required for the flow to exhibit a symmetric velocity profile, as shown in the upstream tangent.

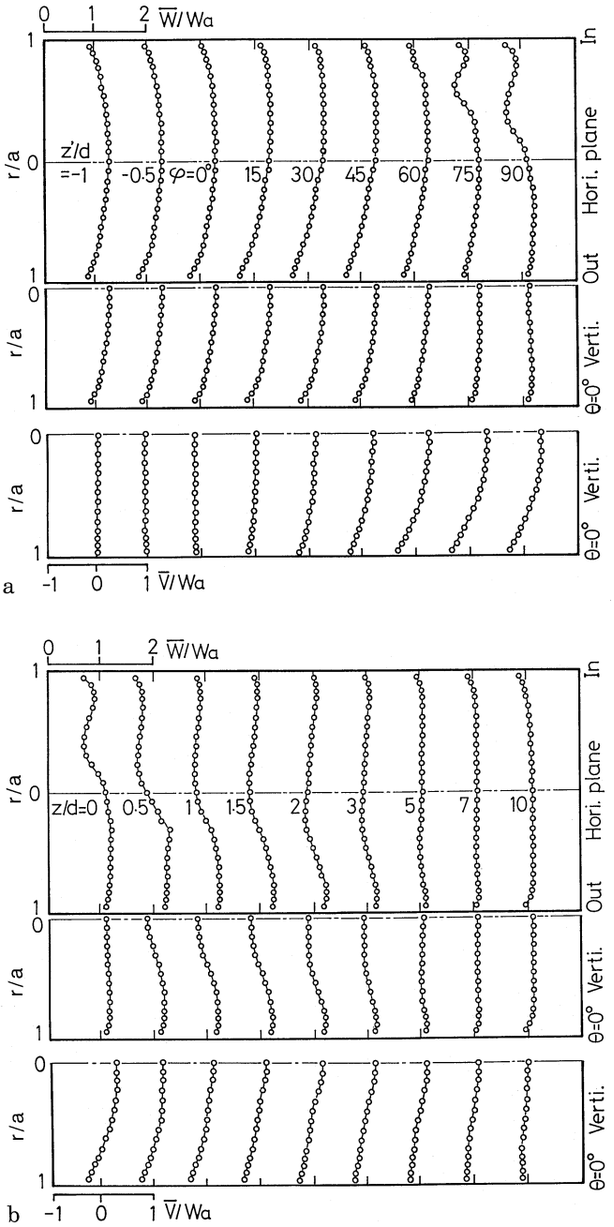

Fig. 4a, b. Distribution of time mean velocity (Top and middle figures: Longitudinal velocity $\bar{W}$ in horizontal and vertical planes respectively. Bottom figure: circumferential velocity $\bar{V}$ in vertical plane). **a** Upstream tangent and bend; **b** downstream tangent

3.2 Reynolds stresses

In this section, we discuss three components of Reynolds stress, $\overline{w'^2}$, $\overline{w'u'}$, and $\overline{v'w'}$, which significantly influence the mean flow characteristic.

Turbulence intensity and its production rate in the longitudinal direction are presented in the form of contours in Fig. 6, where the production rate of turbulence, P_{ww}, can be expressed as

$$P_{ww}=-2\left\{\overline{w'u'}\frac{\partial\bar{W}}{\partial r}+\overline{v'w'}\frac{1}{r}\frac{\partial\bar{W}}{\partial\theta}+\frac{\overline{w'^2}}{h}\times\left(\frac{\partial\bar{W}}{\partial\varphi}+\bar{U}\sin\theta+\bar{V}\cos\theta\right)\right\}, \quad (1)$$

where $h=R_c+r\sin\theta$. At $z'/d=-1$, the turbulence intensity is distributed in axisymmetrically like the mean longitudinal

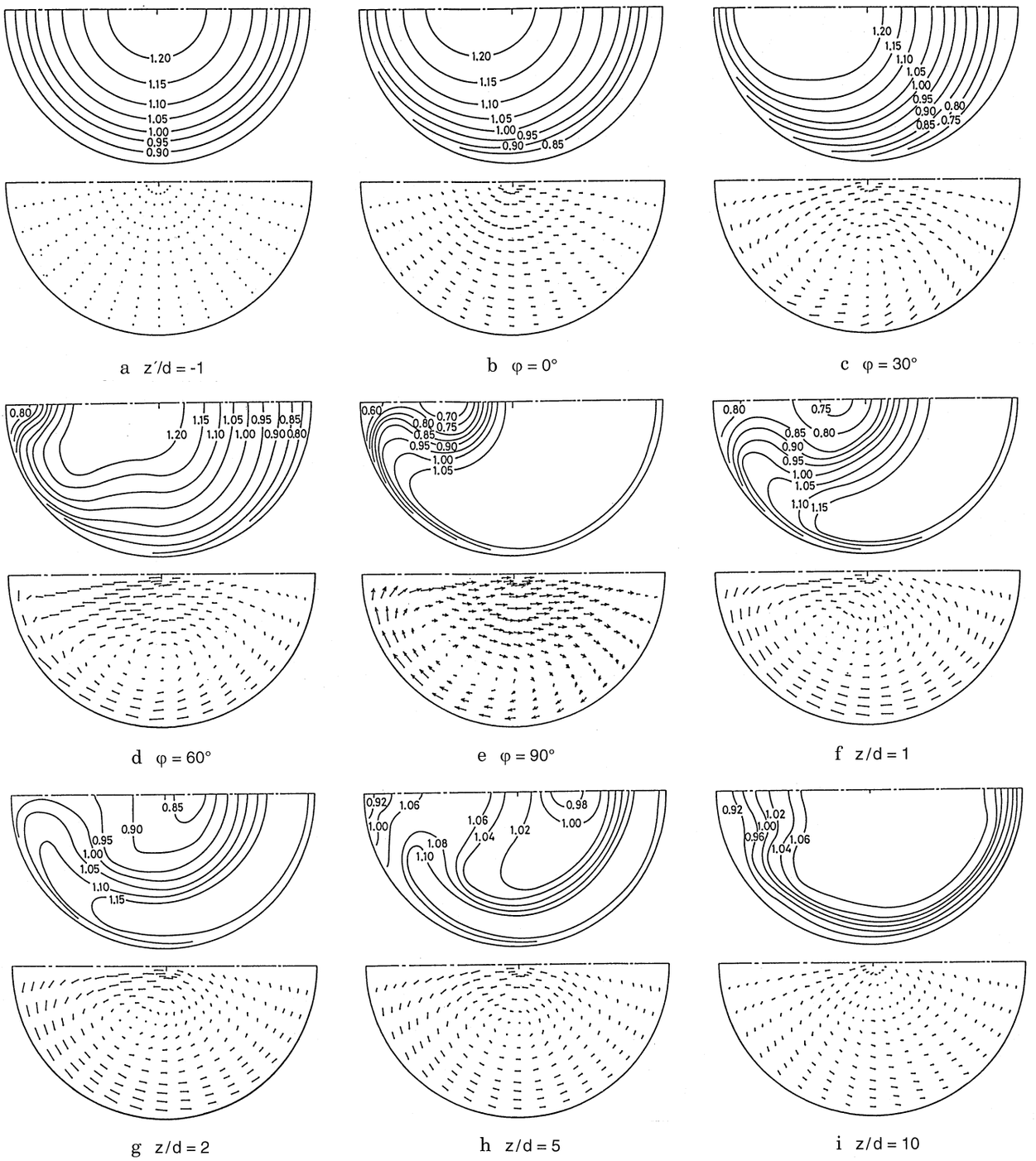

Fig. 5a–i. Time mean flow velocities in cross section. (Top figure: Longitudinal velocity contours, where numerical values are for $\bar{W}/Wa$. Bottom figure: secondary flow velocity vectors, where the length of d/8 corresponds to *Wa*. The left and right sides of each figure show the inside and outside walls in the bend, respectively)

velocity, and the influence of the bend cannot be observed. From $\varphi = 0^\circ$ to $\varphi = 30^\circ$, the turbulence intensity increases in the outer part of the cross section in response to a slight increase of the longitudinal velocity gradients in the radial direction, $\partial\bar{W}/\partial r$, there. At $\varphi = 60^\circ$, a region with high values of turbulence intensity is observed in the vicinity of the inner wall coinciding with large longitudinal velocity gradient, $\partial\bar{W}/\partial r$, near the inner wall. At the bend exit, $\varphi = 90^\circ$, the extremely strong fluctuation is locally produced around the region of the depression of the mean velocity near the inner wall shown in

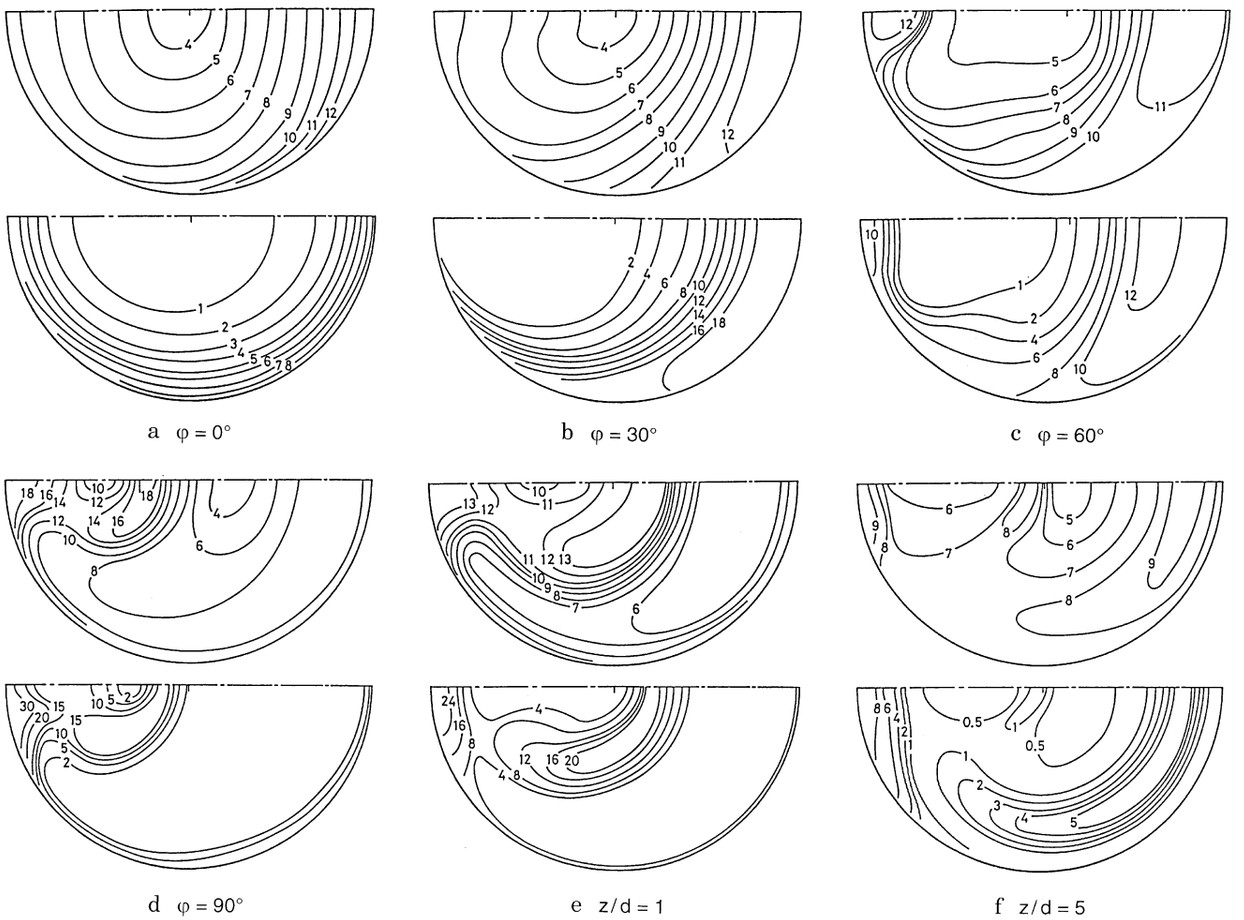

Fig. 6a–f. Turbulence intensity $\overline{w'^2}$ and its production rate P_{ww}. (Top figure: contours of $\sqrt{\overline{w'^2}}/Wa \times 10^2$, bottom figure: contours of $P_{ww} \cdot d/Wa^3 \times 10^3$)

the velocity contours, owing to the steep velocity gradients, and its maximum intensity takes a value of approximately 18%. On the other hand, the weak fluctuation region is extensive in the outer part of the cross section since the longitudinal velocity gradient there is gentle. For $z/d = 0.5$ to 2, however, the intensive turbulence region near the inner wall moves towards the outer part of the cross section along the symmetric plane, corresponding to the shift of the low longitudinal velocity region towards the outer wall. Meanwhile, the region of turbulence with low values detected on the side of the outer wall at the preceding stations is transported towards the inner wall along the upper and lower walls, like the fast longitudinal velocity region. Hence the weak turbulence region near the outer wall disappears at $z/d = 2$ and the gradient of turbulence intensity over the cross section turns out to be relatively gentle. At $z/d = 10$, the weak fluctuation region extends widely over the cross section since the longitudinal velocity distribution becomes flat. However, the contours of turbulence intensity are not concentric and the influence of the bend still remains at this station.

The contours of Reynolds stresses, $\overline{w'u'}$ and $\overline{v'w'}$, and their production rates, P_{wu} and P_{vw}, are shown in Figs. 7 and 8, respectively. Here P_{wu} and P_{vw} can be expressed as

$$P_{wu} = -\left[\overline{u'^2}\frac{\partial \bar{W}}{\partial r} + \overline{w'u'}\left\{\frac{\partial \bar{U}}{\partial r} + \frac{1}{h}\left(\frac{\partial \bar{W}}{\partial \varphi} + \bar{U}\sin\theta + \bar{V}\cos\theta\right)\right\} + \frac{\overline{w'^2}}{h}\left(\frac{\partial \bar{U}}{\partial \varphi} - \bar{W}\sin\theta\right) + \overline{v'w'}\left(\frac{1}{r}\frac{\partial \bar{U}}{\partial \theta} - \frac{\bar{V}}{r}\right)\right] \quad (2)$$

$$P_{vw} = -\left[\frac{\overline{v'^2}}{r}\frac{\partial \bar{W}}{\partial \theta} + \overline{v'w'}\left\{\left(\frac{1}{r}\frac{\partial \bar{V}}{\partial \theta} + \frac{\bar{U}}{r}\right) + \frac{1}{h}\left(\frac{\partial \bar{W}}{\partial \varphi} + \bar{U}\sin\theta + \bar{V}\cos\theta\right)\right\} + \frac{\overline{w'^2}}{h}\left(\frac{\partial \bar{V}}{\partial \varphi} - \bar{W}\cos\theta\right) + \overline{w'u'}\frac{\partial \bar{V}}{\partial r}\right] \quad (3)$$

At the bend inlet, $\varphi = 0°$, the correlation $\overline{v'w'}$ is generated, even though it is slightly weak, by the circumferential gradient of the longitudinal velocity, $\partial \bar{W}/\partial \theta$, which is induced by an acceleration and deceleration of the primary flow near the inner and outer walls. At $\varphi = 30°$, the correlation $\overline{v'w'}$, which has a negative value, increases over the cross section, according to the large circumferential velocity gradient, $\partial \bar{W}/\partial \theta$. Reversely,

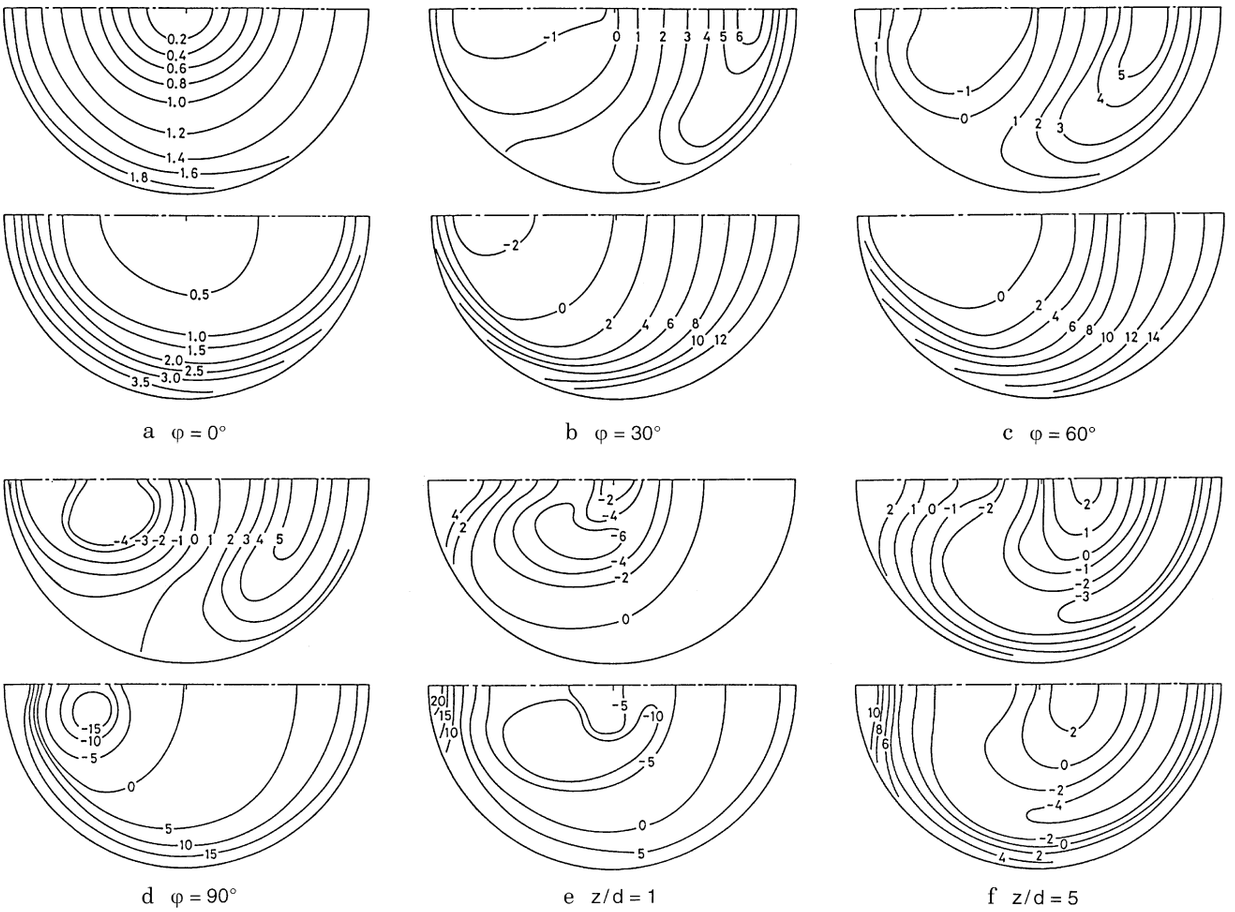

Fig. 7a–f. Reynolds stress $\overline{w'u'}$ and its production rate P_{wu}. (Top figure: contours of $\overline{w'u'}/Wa^2 \times 10^2$, bottom figure: contours of $P_{wu} \cdot d/Wa^2 \times 10^3$)

the Reynolds stress $\overline{w'u'}$ diminishes in the inner part of the cross section, because of the decrease of the radial velocity gradient, $\partial\bar{W}/\partial r$, as seen in Fig. 5c. At the bend exit, $\varphi = 90^\circ$, both $\overline{w'u'}$ and $\overline{v'w'}$ indicate high absolute values near the inner wall in accordance with the large velocity gradients, $\partial\bar{W}/\partial r$ and $\partial\bar{W}/\partial\theta$, around the low-velocity region near the inner wall. Between $z/d = 0$ and 2, the regions of positive $\overline{v'w'}$ and of negative $\overline{w'u'}$ shift towards the outer part with the shift of the steep velocity gradient region towards the outer part, and they exhibit complicated contours. At $z/d = 5$, the region of negative $\overline{v'w'}$ surrounded by positive $\overline{v'w'}$ extends to the central part of the cross section. The signs of correlations $\overline{v'w'}$ correspond to those of the velocity gradient $\partial\bar{W}/\partial\theta$. At a station further downstream, $z/d = 10$, the degrees of both correlation decrease as the profile of the longitudinal velocity becomes smooth.

3.3
Characteristic quantities of the bend flow

In order to estimate the variation of flow characteristics, such as the deviation of primary flow, the intensity of secondary flow and the turbulence energy along the longitudinal distance, the following quantities averaged over the cross section of the bend are introduced:

$$\bar{x}/d = \frac{8}{\pi d^2\, Wa} \int_{-\pi/2}^{\pi/2} \int_{0}^{a} \left(\frac{r \sin\theta}{d}\right) \bar{W} r \, \mathrm{d}r \, \mathrm{d}\theta \tag{4}$$

$$I_s = \frac{8}{\pi d^2\, Wa^2} \int_{-\pi/2}^{\pi/2} \int_{0}^{a} (\bar{U}^2 + \bar{V}^2)\, r \, \mathrm{d}r \, \mathrm{d}\theta \tag{5}$$

$$k_a = \frac{8}{\pi d^2\, Wa^2} \int_{-\pi/2}^{\pi/2} \int_{0}^{a} \frac{1}{2} (\overline{u'^2} + \overline{v'^2} + \overline{w'^2})\, r \, \mathrm{d}r \, \mathrm{d}\theta \tag{6}$$

The results estimated using Eqs. (4)–(6) are shown in Fig. 9. The primary flow starts to deflect towards the inner wall at the front of the bend inlet and deflects most to the inside of the bend near $\varphi = 30^\circ$. Thereafter the deviation of primary flow turns towards the outer wall and the flow continues to deflect towards the outer side of the bend to a considerably downstream station. The secondary flow occurs at the vicinity of the bend inlet and becomes strongest at the bend exit $\varphi = 90^\circ$. Although the intensity of secondary flow decreases rapidly in the downstream tangent, the secondary flow can be recognized even at $z/d = 10$. The turbulence energy begins to increase near the bend inlet and is the highest between the

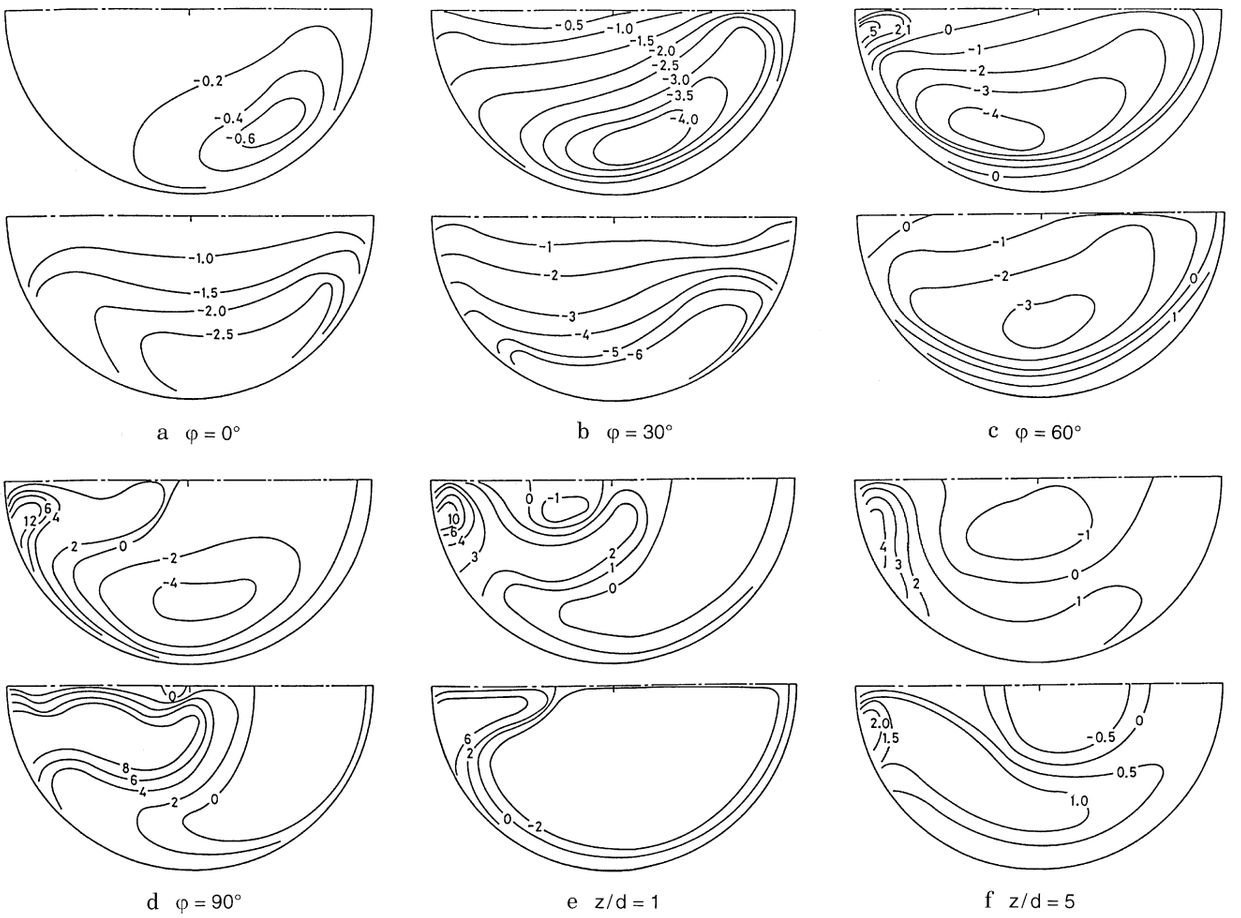

Fig. 8a–f. Reynolds stress $\overline{v'w'}$ and its production rate P_{vw}. (Top figure: contours of $\overline{v'w'}/Wa^2 \times 10^2$, bottom figure: contours of $P_{vw} \cdot d/Wa^3 \times 10^3$)

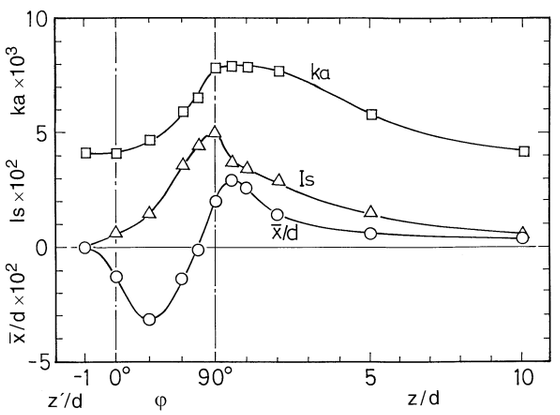

Fig. 9. Longitudinal variation of cross-sectional average quantities

bend exit and the downstream station, $z/d = 0.5$. Subsequently, it slowly returns to the value of straight pipe flow.

4 Conclusions

Concerning the turbulent flow in the circular-sectioned 90° bend with long upstream and downstream tangents, the following were clarified.

(1) In the inlet region of the bend, the primary flow accelerates near the inner wall and a secondary flow moving from the outer to the inner wall of the bend occurs in the bend cross section.

(2) At station $\varphi = 30°$ in the bend, the secondary flow develops into a pair of vortices, as seen in fully developed curved pipe flows, but the primary flow remains deflected toward the inner wall. The Reynolds stress $\overline{w'u'}$ tends to decrease in the inner part of the cross section and $\overline{v'w'}$ increases in the outer part.

(3) Between $\varphi = 75°$ and 90°, the velocity contours of primary flow are greatly distorted and a depression in the contour plot is formed in the inner part of the bend cross section. The turbulence intensity and the Reynolds stresses increase around the depression of contours, coinciding with the large velocity gradient there.

(4) Just behind the bend exit, the primary flow velocity in the central region of the pipe decreases and the correlations of fluctuating velocities exhibit a complicated distribution according to the variation of primary flow velocity profiles.

(5) At successive downstream stations, the distribution of primary flow velocity gradually becomes smooth. The secondary flow weakens and vortices break down. The influence of the bend on the flow, however, remains even at $z/d = 10$.

The present data are useful for checking the validity of mathematical models of turbulence. To gain further knowledge, future work is required for flows in bends with different degrees of turn, for example, 180°.

References

ANC1/ASME PTC 19.1-1985 (1987) Measurement uncertainty, Supplement on instruments and apparatus (translated by JSME, p 26, Tokyo: Maruzen

Azzola J; Humphrey JAC; Iacovides H; Launder BE (1986) Developing turbulent flow in a U-bend of circular cross-section: measurement and computation. Trans ASME: J Fluid Eng 108: 214–221

Chang SM; Humphrey JAC; Modavi A (1983) Turbulent flow in a strongly curved U-bend and downstream tangent of square cross-sections. Physico-Chemical Hydrodynamics 4: 243–269

Enayet MM; Gibson MM; Taylor AMKP; Yianneskis M (1982) Laser-doppler measurements of laminar and turbulent flow in a pipe bend. Int J Heat and Fluid Flow 3: 213–219

Humphrey JAC; Whitelaw JH; Yee G (1981) Turbulent flow in a square duct with strong curvature. J Fluid Mech 103: 443–463

Laufer J (1954) The structure of turbulence in fully developed pipe flow. NACA Technical Report No. 1174

Sudo K; Takami T; Hibara H (1992) Velocity measurement in three-dimensional turbulent flows by rotating a probe with an inclined hot wire (in Japanese). Trans Jpn Soc Mech Eng 58: 379–385

Taylor AMKP; Whitelaw JH; Yianneskis M (1982) Curved ducts with strong secondary motion: velocity measurements of developing laminar and turbulent flow. Trans ASME: J Fluid Eng 104: 350–359